

## Two-dimensional chiral asymmetry in unidirectional magnetic anisotropy structures

P. Perna,<sup>1,a</sup> F. Ajejas,<sup>1,2</sup> D. Maccariello,<sup>1,2</sup> J. L. Cuñado,<sup>1,2</sup> R. Guerrero,<sup>1</sup> M. A. Niño,<sup>1</sup> M. Muñoz,<sup>3,4</sup> J. L. Prieto,<sup>4</sup> R. Miranda,<sup>1,2,5</sup> and J. Camarero<sup>1,2,5</sup>

<sup>1</sup>IMDEA-Nanoscience, c/ Faraday, 9 Campus de Cantoblanco, 28049 Madrid, Spain

<sup>2</sup>DFMC and Instituto “Nicolás Cabrera”, Universidad Autónoma de Madrid, 28049 Madrid, Spain

<sup>3</sup>IMM-CSIC, Isaac Newton 8, PTM, 28760 Tres Cantos, Madrid, Spain

<sup>4</sup>ISOM, Universidad Politécnica de Madrid, 28040 Madrid, Spain

<sup>5</sup>Condensed Matter Physics Center (IFIMAC), Universidad Autónoma de Madrid, 28049 Madrid, Spain

(Presented 15 January 2016; received 5 November 2015; accepted 8 January 2016; published online 11 March 2016)

We investigate the symmetry-breaking effects of magnetic nanostructures that present unidirectional (one-fold) magnetic anisotropy. Angular and field dependent transport and magnetic properties have been studied in two different exchange-biased systems, i.e. ferromagnetic (FM)/ antiferromagnetic (AFM) bilayer and spin-valve structures. We experimentally show the direct relationships between the magnetoresistance (MR) response and the magnetization reversal pathways for any field value and direction. We demonstrate that even though the MR signals are related to different transport phenomena, namely anisotropic magnetoresistance (AMR) and giant magnetoresistance (GMR), chiral asymmetries are found around the magnetization hard-axis direction, in both cases originated from the one-fold symmetry of the interfacial exchange coupling. Our results indicate that the chiral asymmetry of transport and magnetic behaviors are *intrinsic* of systems with an unidirectional contribution. © 2016 Author(s). All article content, except where otherwise noted, is licensed under a Creative Commons Attribution 3.0 Unported License. [<http://dx.doi.org/10.1063/1.4944345>]

Chirality is a symmetry property found in many branches of science. Even though it is often referred to three-dimensional (3D) objects (human hand, molecules), Lord Kelvin's definition was not limited to the 3D case by defining as chiral any object for which “its image in a plane mirror cannot be brought to coincide with itself”.<sup>1</sup> In magnetism, the handedness of the magnetization vector and the external field result most often with non-chiral hysteresis phenomena,<sup>2</sup> i.e., its mirror image can be superposed upon series of rotations and/or translations. Recently, it has been found that interfacial symmetry-breaking can promote chiral phenomena, including magnetic<sup>3,4</sup> and magnetoresistance<sup>4</sup> properties.

The purpose of this paper is to give a general picture on the chiral asymmetry properties of exchange-biased magnetic nanostructures. In particular, they present chiral asymmetries around the magnetization hard-axis (h.a.) direction in both transport and magnetic properties. We demonstrate that such asymmetry is determined by the unidirectional (one-fold) magnetic anisotropy imposed by the interfacial exchange coupling at the ferromagnetic/antiferromagnetic (FM/AFM) interface. In order to prove that this is a general behavior, we have considered two exchange-biased systems, i.e. FM/AFM bilayer and spin-valve structure, as illustrated in Fig. 1, in which the MR signals are related to different phenomena, i.e. anisotropic magnetoresistance (AMR) and giant magnetoresistance (GMR) respectively.

<sup>a</sup>paolo.perna@imdea.org

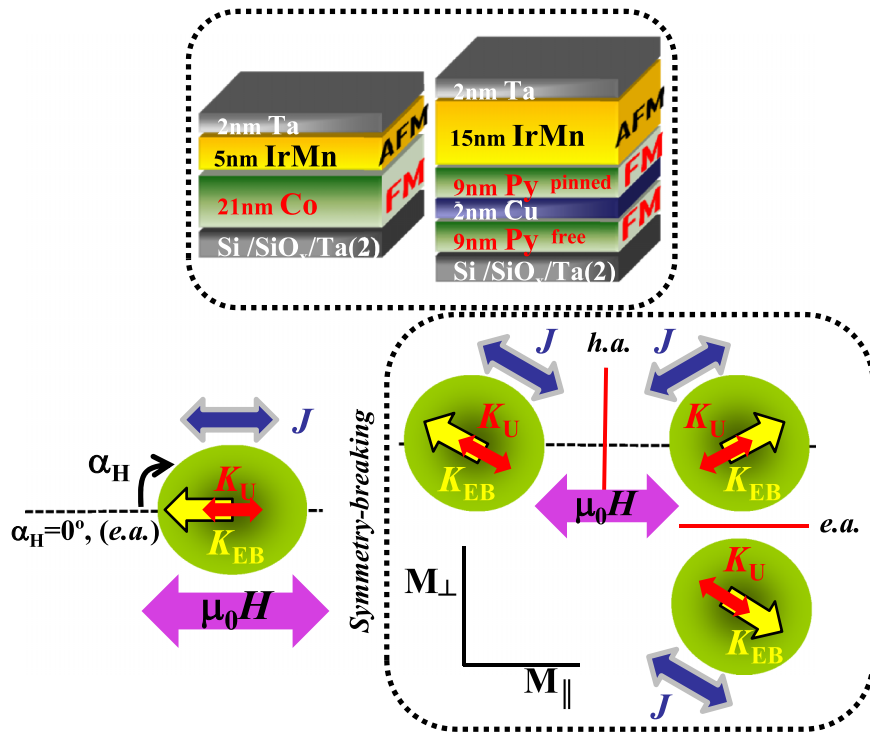


FIG. 1. Schemes of the FM/AFM and exchange-bias spin-valve structures (top-box). The system magnetic anisotropy configuration (collinearity between uniaxial magnetic anisotropy  $K_U$  of the FM layer and unidirectional magnetic anisotropy  $K_{EB}$  imposed by the AFM) is shown on the bottom. The experimental parameters are also illustrated:  $M_{\parallel}$  and  $M_{\perp}$  are the in-plane components of the magnetization, parallel and perpendicular to the external magnetic field ( $\mu_0 H$ ), being  $\alpha_H$  the angle enclosed between  $\mu_0 H$  and the uniaxial anisotropy  $K_U$  of the FM. The electrical current  $J$  is injected parallel to  $K_U$ . The right box illustrates the configuration around the h.a. direction in which the chiral asymmetry of the MR curves is observed.

The AMR depends on  $\cos^2 \theta$ , being  $\theta$  the angle enclosed by the injected electrical current ( $J$ ) and the magnetization ( $M$ ) of the system, and arises from spin-orbit interaction.<sup>5,6</sup> On the other hand, the GMR depends on the angle  $\phi$  between the magnetization vectors of two FM layers separated by a non-magnetic (NM) metal, and follows a  $\cos \phi$  behavior.<sup>7,8</sup> Such an effect originates from bulk spin-dependent scattering processes affecting electrons that travel across the structure.<sup>9</sup>

In general, FM/AFM structures are employed in order to stabilize the MR output in sensing and memory spintronic applications. In these systems, the magnetization direction of the FM is pinned by the interfacial coupling imposed by the adjacent AFM layer<sup>10</sup> determining a shift of the hysteresis loop of the FM layer (exchange-bias (EB) field) and an enhancement of the coercivity. The EB introduces hence an additional unidirectional magnetic anisotropy giving rise to different features depending strongly on the applied field angle  $\alpha_H$ , including magnetization reversal pathways<sup>11</sup> and MR responses.<sup>4</sup> Exchange-biased spin-valve structures are composed of two FM electrodes, one of them pinned with an AFM layer, separated by a NM spacer.<sup>12</sup> In this case, for some specific angles, the free FM layer can reverse its magnetization while the magnetization of the FM adjacent to the AFM is kept fixed. These FM(free)/NM/FM(pinned)/AFM structures exhibit GMR response that depends strongly on the applied field angle  $\alpha_H$ .<sup>13</sup>

The systems are fabricated by dc magnetron sputtering at room temperature (RT) on thermally oxidized Si substrates capped with a 2-nm thick Ta buffer. The layer sequence are Co (22 nm) / IrMn (5 nm) for the FM/AFM bilayer, and Ni<sub>80</sub>Fe<sub>20</sub>(9 nm)/Cu(2 nm)/Ni<sub>80</sub>Fe<sub>20</sub>(9 nm)/FeMn(15 nm) for the spin-valve. The samples are finally capped by 2 nm of Ta to prevent oxidation. In order to set a defined two-fold (uniaxial) magnetic anisotropy ( $K_U$ ) of the FM layers and to induce a one-fold (collinear) unidirectional anisotropy ( $K_{EB}$ ), the samples were grown in an in-plane magnetic field of 200 mT (Fig. 1). The magnetic and transport characterizations have been performed at room

temperature (RT) at different applied field angles  $\alpha_H$  by using a M(R)OKE set-up,<sup>4,13,14</sup> which allows the *simultaneous* acquisition of MR and vectorial-resolved magnetization curves.<sup>15</sup>  $\alpha_H$  is the sample in-plane angular rotation angle, keeping fixed the external magnetic field direction  $\mu_0 H$ , and  $\alpha_H = 0^\circ$  is taken when the external field is aligned parallel to the direction of  $K_U$ , i.e. along the easy-axis (e.a.) of the system (Fig. 1). To measure MR, we have employed an ac technique in which  $\mathbf{J}$  is injected parallel to  $K_U$ . The samples were contacted using Au-wire bonding in four-probe current-in-plane geometry. The samples resistance was about 10-20  $\Omega$ . MR was calculated through the experimental  $R(H)$  curves, i.e.  $MR(H) = \frac{R(H) - R_S}{R_S}$ , where  $R_S$  is the resistance in saturation state. The in-plane magnetization components (parallel  $M_{\parallel}$  and perpendicular  $M_{\perp}$  to the external magnetic field) were derived from Kerr curves by using p-polarized light focused between the inner electric probes.<sup>15,16</sup> It is worth remarking that in our vectorial-resolved experiments we get direct access to the sample magnetization vector through the angle  $\alpha \equiv (\mathbf{M}, \mathbf{H})$  that defines the magnetic torque ( $\propto \sin \alpha$ ).<sup>14</sup>

In Fig. 2 the simultaneous MR-H and  $M_{\parallel}$ -H loops at the e.a. direction are presented for both structures. In the case of the FM/AFM bilayer in Fig. 2(a), the MR signal is flat and constant in the whole field loop, like in a single FM layer.<sup>14</sup> This is due to invariance of the angle between  $\mathbf{M}$  and  $\mathbf{J}$ .<sup>4</sup> In fact, the magnetization is always parallel to the external field, as observed in the  $M_{\parallel}$ -H corresponding bottom-graph, which displays squared hysteresis with sharp transitions from one saturation state to the other. The hysteresis is shifted of  $\mu_0 H_{EB} = +4.7$  mT because of the exchange-bias effect. The maximum MR variation is 0.13%.

In the case of spin-valve in Fig. 2(b), at the e.a. the MR curve presents sharp transitions between low and high resistance states, and well-defined plateaus. These correspond to the parallel and antiparallel alignment of the magnetization of the two FM electrodes, as demonstrated by the simultaneous M-H loop (bottom-graph).<sup>13</sup> In the latter, it is possible to discriminate two distinctive hysteresis loops due to the free-FM reversal (with smaller coercivity), and the one due to the pinned-FM shifted towards higher field value ( $\mu_0 H_{EB} = +7$  mT).<sup>17,18</sup> The maximum MR value is found at the e.a. and is 2.3%.

Around the h.a. direction similar symmetric relationships are observed in both MR and magnetization loops appear for both structures.

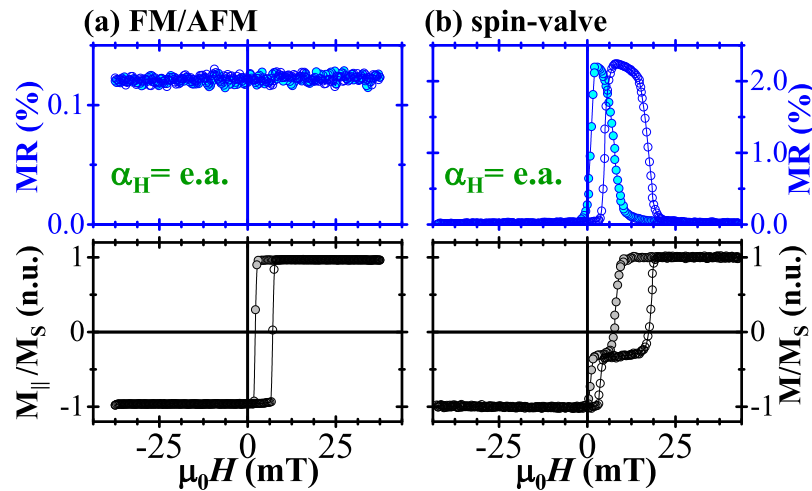


FIG. 2. (a) Field-dependent MR and magnetization ( $M_{\parallel}/M_S$ , where  $M_S$  is the saturation magnetization) loops of FM/AFM bilayer at  $\alpha_H = \text{e.a.}$  Since  $\mathbf{M}$  is forced to be parallel to the field in the whole loop,  $\theta$  does not change and the MR is flat and constant. This is clearly seen through the M-H loop in the corresponding bottom panel. (b) Field-dependent MR and magnetization ( $M_{\parallel}/M_S$ , where  $M_S$  is the saturation magnetization) loops of the exchange-bias spin-valve at  $\alpha_H = \text{e.a.}$  The MR curve presents sharp transitions between low and high resistance states, an well-defined plateaus corresponding to the parallel and antiparallel magnetization configuration of the two FM electrodes, as demonstrating by the simultaneous M-H loop (bottom-panel). In the latter, the hysteresis curve with smaller coercivity is ascribed to the free-FM, whereas the shifted loops is due to the pinned-FM. Filled (empty) symbols refers to descending (ascending) branch.

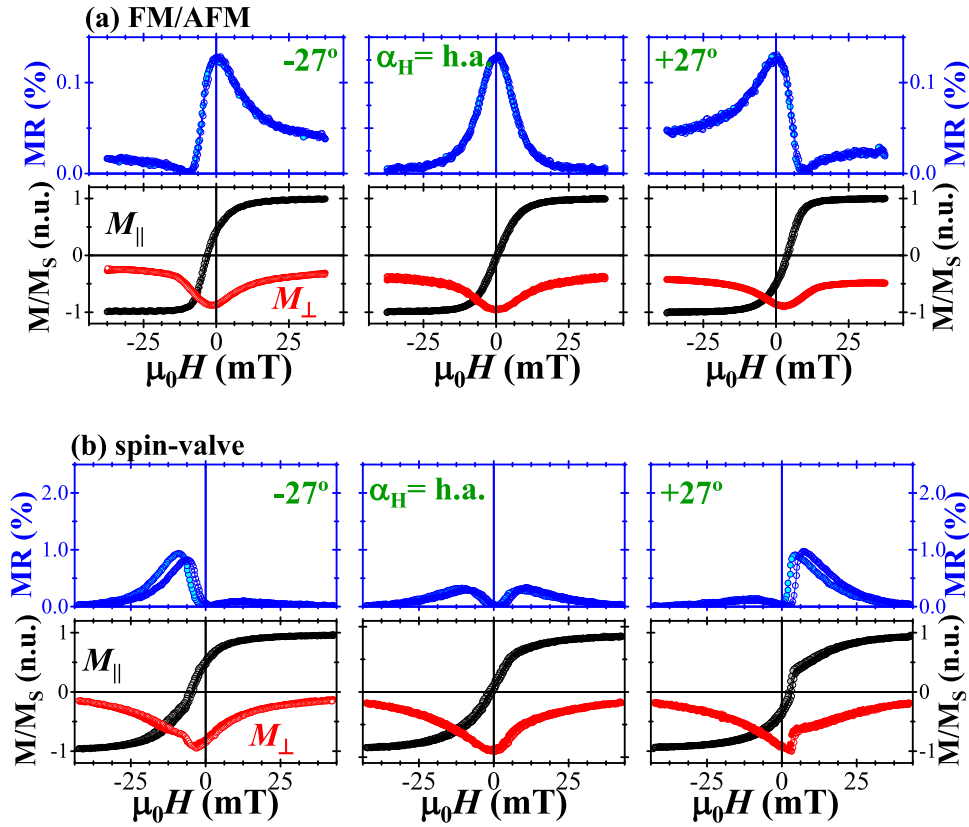


FIG. 3. (a) Field-dependent MR (top-graphs) and magnetization (bottom-graphs) loops of FM/AFM bilayer at selected angles  $\alpha_H$  around h.a. (i.e.,  $\alpha_H = \text{h.a.} \pm 27^\circ$ ). Exactly at h.a., the MR presents the maximum variation since at high field (saturation)  $\mathbf{M}$  and  $\mathbf{J}$  are parallel, whereas at smaller field the magnetization rotates trying to be aligned to the anisotropy direction. This is demonstrated by the field-loop of the two in-plane magnetization components ( $M_{\parallel}$  and  $M_{\perp}$ ). (b) Field-dependent MR (top-graphs) and magnetization (bottom-graphs) loops of spin-valve around h.a.,  $\alpha_H = \text{h.a.} \pm 27^\circ$ . In contrast to the sharp transition found in the e.a. region, smoother transitions (in both MR and magnetization loops) become progressively more relevant as approaching to the h.a. direction (reversal dominated by magnetization rotation mechanisms). As consequence, the maximum MR value is minimum exactly at h.a. Filled (empty) symbols refers to descending (ascending) branch. Note the chiral asymmetry displayed by the MR and  $M_{\perp}$  curves around the h.a., i.e.  $\alpha_H = \text{h.a.} \pm 27^\circ$ .

As shown in Fig. 3(a), 3(b), in both cases the MR signals (top-graphs) are symmetric with respect to the zero-field only exactly at the h.a., while around it, i.e.  $\alpha_H = \text{h.a.} \pm 27^\circ$ , the MR-H curves are strongly asymmetric and chiral. Moreover, they change accordingly to the magnetization loops ( $M_{\parallel}$ -H and  $M_{\perp}$ -H in the corresponding bottom-graphs). This is due to the occurrence of different magnetization reversal processes. In fact, while in the e.a. region, the reversal proceeds by nucleation and further propagation of magnetic domains (squared loops and sharp transitions in Fig. 2(a), 2(b)), approaching to the h.a., reversible transitions become more important.<sup>16,19</sup> This is seen in the  $M_{\parallel}$  and  $M_{\perp}$  curves characterized by smooth transitions (with no hysteresis) indicating that magnetization rotation is the relevant process during reversal. In particular, exactly at the h.a.,  $M_{\parallel}$ -H displays a nearby linear behavior ( $\mu_0 H_C \approx 0$  mT) in both systems, while  $M_{\perp}$  is always negative. These features indicate that, during the reversal, the magnetization rotates in-plane only in one semi-circle because of the unidirectional anisotropy. Analogously to MR-H, also  $M_{\perp}$  curves present chiral asymmetry around the h.a. In particular, while around the e.a. direction magnetoresistance and magnetization curves show identical behaviors,<sup>4,13</sup> around the h.a. MR-H and  $M_{\perp}$ -H present chiral asymmetry. In fact,  $M_{\perp}(\text{h.a.} + 27^\circ, H) = M_{\perp}(\text{h.a.} - 27^\circ, -H)$  and  $\text{MR}(\text{h.a.} + 27^\circ, H) = \text{MR}(\text{h.a.} - 27^\circ, -H)$ , whereas  $M_{\parallel}(\text{h.a.} + 27^\circ, H) = -M_{\parallel}(\text{h.a.} - 27^\circ, -H)$ .

However, since the magnetoresistive signals of the two systems are related to different phenomena, the MR-H curve shape and maximum value present important differences as well.

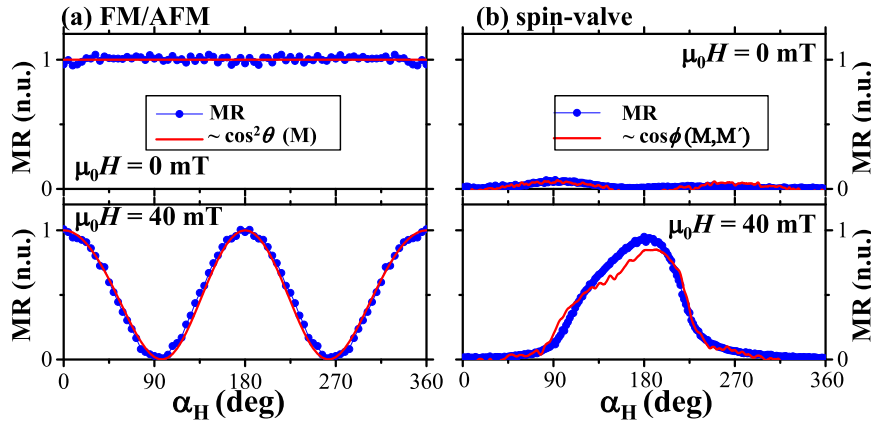


FIG. 4. Angular evolution of the MR at selected field values for (a) FM/AFM and (b) spin-valve. In the first case, the MR depends on  $\cos^2 \theta$ . In the latter case, the MR is proportional to  $\cos \phi$ .  $\cos^2 \theta$  and  $\cos \phi$  determined through the measured magnetization components and their angular behaviors are superimposed to the corresponding experimental MR data in order to demonstrate their similarities.

In the FM/AFM case shown in Fig. 3(a), approaching to the hard direction, the MR jump becomes larger and larger and it is maximum exactly at the h.a. In fact, as the field is misaligned with the anisotropy direction, the magnetization vector rotates and the MR-H curves change accordingly (the angle between  $\mathbf{M}$  and  $\mathbf{J}$  varies). Exactly at the h.a., sweeping the field  $\mathbf{M}$  rotates in-plane, and therefore the MR assumes the minimum (maximum) value at saturation field (zero-field) since  $\mathbf{M}$  points perpendicularly to the current direction ( $\mathbf{M}$  tries to be aligned to  $K_U$ ). As mentioned above, in spin-valves (Fig. 3(b)), MR depends on the relative orientation ( $\phi$ ) of the magnetization vectors of the two FM electrodes. As the field is misaligned with respect to the anisotropy axis, the MR curves present smoother transitions related to different configuration of the magnetization of the FM layers. The maximum value of MR decreases progressively as approaching to the h.a. direction (reversal dominated by rotation processes). Exactly at the h.a. only reversible transitions occur and we find the lowest resistivity variation of the whole angular cycle (central graph). To note that a AMR contribution would be expected from the whole structure, but it is much smaller than the GMR effect.

The vectorial-Kerr experiments allow us to determine the angles  $\theta \equiv (\widehat{\mathbf{M}}, \mathbf{J})$  and  $\phi \equiv (\widehat{\mathbf{M}'}, \widehat{\mathbf{M}''})$  (where  $\mathbf{M}'$  and  $\mathbf{M}''$  are the magnetization vectors of the two FMs) for any values and direction of the applied magnetic field  $\mu_0 H$  for both structures. In such a way we are able to compare the experimental  $R(H)$  curves with the calculated  $\cos^2 \theta (M_{\parallel}, M_{\perp})$ <sup>4,14</sup> and  $\cos \phi ((M'_{\parallel}, M'_{\perp}), (M''_{\parallel}, M''_{\perp}))$ ,<sup>13</sup> the current direction being fixed (and parallel to  $K_U$ ). Therefore the chiral MR asymmetry we observe is not due to any spin Hall effects.<sup>20,21</sup> In fact, in Fig. 4 we present the angular evolution of AMR and  $\cos^2 \theta$  for FM/AFM [in panel (a)] and GMR and  $\cos \phi$  for spin-valve [in panel (b)]. For simplicity, only two representative field values are plotted, which are zero-field and  $\mu_0 H = 40$  mT (close to saturation). In the former case, the perfect agreement between the experimental AMR data and  $\cos^2 \theta$  demonstrates the dependence (for any field value and direction) of the MR response on  $(\widehat{\mathbf{M}}, \mathbf{J})$ . Analogously, in spin-valve the GMR behaviors can be reproduced satisfactorily by the cos of the angle between the two FM electrodes.

In conclusion, we have shown that even though the MR signals in the two structures are related to different phenomena (AMR in FM/AFM bilayer and GMR in spin-valve), around the magnetization hard direction they display chiral asymmetry. This is due to the additional (one-fold) unidirectional magnetic anisotropy imposed by the FM/AFM core-stack via interfacial exchange coupling. Generalizing, any system in which a unidirectional anisotropy is present displays asymmetric signals (usually observed at small magnetic field).<sup>3,22–24</sup> Our data confirm that broken surface/interface symmetry due to (unidirectional) exchange-bias causes chirality in both MR and magnetization curves in low-dimensional magnetic structures with in-plane magnetic anisotropy.

This work was supported in part by the Spanish MINECO through Project No. MAT2012-39308, FIS2013-40667-P and MAT2014-52477-C5-3-P, and by the Comunidad de Madrid through

Project S2013/MIT-2850 (NANOFrontMAG-CM). P.P. acknowledges support through Marie Curie AMAROUT EU Programme and JCI-2011-09602.

- <sup>1</sup> Sir William Thomson Lord Kelvin, *The Molecular Tactics of a Crystal* (Clarendon Press, 1894).
- <sup>2</sup> G. Bertotti, *Hysteresis in magnetism* (Academic Press, 1998).
- <sup>3</sup> S. Pizzini *et al.*, *Phys. Rev. Lett.* **113**, 047203 (2014).
- <sup>4</sup> P. Perna, F. Ajejas, D. Maccariello, J. L. Fernandez Cuñado, R. Guerrero, M. A. Niño, A. Bollero, R. Miranda, and J. Camarero, *Phys. Rev. B* **92**, 220422(R) (2015).
- <sup>5</sup> I. A. Campbell and A. Fert, in *Ferromagnetic Materials*, edited by E. P. Wohlfarth (North-Holland, Amsterdam, 1982), Vol. 3.
- <sup>6</sup> T. R. McGuire and R. I. Potter, *IEEE Trans. Magn.* **11**, 1018 (1975).
- <sup>7</sup> L. B. Steren, A. Barthelemy, J. L. Duvail, A. Fert, R. Morel, F. Petroff, P. Holody, R. Loloee, and P. A. Schroeder, *Phys. Rev. B* **51**, 292 (1995).
- <sup>8</sup> G. E. W. Bauer, Y. Tserkovnyak, D. Huertas-Hernando, and A. Brataas, *Phys. Rev. B* **67**, 094421 (2003).
- <sup>9</sup> M.N. Baibich, J.M. Broto, A. Fert, F. Nguyen Van Dau, F. Petroff, P. Eitenne, G. Creuzet, A. Friederich, and J. Chazelas, *Phys. Rev. Lett.* **61**, 2472 (1988); G. Binasch, P. Grünberg, F. Saurenbach, and W. Zinn, *Phys. Rev. B* **39**, 4828 (1989).
- <sup>10</sup> J. Nogues and I. K. Schuller, *J. Magn. Magn. Mater.* **192**, 203 (1999).
- <sup>11</sup> J. Camarero *et al.*, *Phys. Rev. Lett.* **95**, 057204 (2005); E. Jiménez *et al.*, *Appl. Phys. Lett.* **95**, 122508 (2009); E. Jiménez *et al.*, *J. Appl. Phys.* **109**, 07D730 (2011).
- <sup>12</sup> B. Dieny, V.S. Speriosu, S.S.P. Parkin, B.A. Gurney, D.R. Wilhoit, and D. Mauri, *Phys. Rev. B* **43**, 1297 (1991).
- <sup>13</sup> P. Perna, C. Rodrigo, M. Muñoz, J. L. Prieto, A. Bollero, D. Maccariello, J. L. F. Cuñado, M. Romera, J. Akerman, E. Jiménez, N. Mikuszeit, V. Cros, J. Camarero, and R. Miranda, *Phys. Rev. B* **86**, 024421 (2012).
- <sup>14</sup> P. Perna, D. Maccariello, C. Rodrigo, J.L.F. Cuñado, M. Muñoz, J.L. Prieto, M.A. Niño, A. Bollero, J. Camarero, and R. Miranda, *Appl. Phys. Lett.* **104**, 202407 (2014).
- <sup>15</sup> E. Jiménez *et al.*, *Rev. Sci. Instrum.* **85**, 053904 (2014); J. L. Cuñado *et al.*, *Rev. Sci. Instrum.* **86**, 046109 (2015).
- <sup>16</sup> P. Perna *et al.*, *J. Appl. Phys.* **110**, 13919 (2011); *Ibid.*, *J. Appl. Phys.* **109**, 07B107 (2011).
- <sup>17</sup> The residual shift from the zero field of  $\approx +1.2$  mT originates from a magnetostatic “orange-peel” coupling with the pinned-FM layer.<sup>18</sup>
- <sup>18</sup> Y. Pennec, J. Camarero, J.-C. Toussaint, S. Pizzini, M. Bonfim, F. Petroff, W. Kuch, F. Offi, K. Fukumoto, F. Nguyen Van Dau, and J. Vogel, *Phys. Rev. B* **69**, 180402 (2004).
- <sup>19</sup> P. Perna, L. Méchin, M. Saïb, J. Camarero, and S. Flament, *New J. Phys.* **12**, 103033 (2010).
- <sup>20</sup> A. Hoffmann, *IEEE Trans. Magn.* **49**, 5172 (2013).
- <sup>21</sup> H. Nakayama, M. Althammer, Y.-T. Chen, K. Uchida, Y. Kajiwara, D. Kikuchi, T. Ohtani, S. Geprägs, M. Opel, S. Takahashi, R. Gross, G. E. W. Bauer, S. T. B. Goennenwein, and E. Saitoh, *Phys. Rev. Lett.* **110**, 206601 (2013).
- <sup>22</sup> A. N. Bogdanov and U. K. Rößler, *Phys. Rev. Lett.* **87**, 037203 (2001).
- <sup>23</sup> X. Zhou *et al.*, *Sci. Rep.* **5**, 9183 (2015).
- <sup>24</sup> C. Du, H. Wang, F. Yang, and P. C. Hammel, *Phys. Rev. B* **90**, 140407(R) (2014).